# Electrochemically Induced Surface Metal Migration in Well-Defined Core−Shell Nanoparticles and Its General Influence on Electrocatalytic Reactions

Casey N. Brodsky,[†,§] Allison P. Young,[†] Ka Chon Ng,[‡] Chun-Hong Kuo,[‡] and Chia-Kuang Tsung*,[†]

[†]Department of Chemistry, Merkert Chemistry Center, Boston College, 2609 Beacon Street, Chestnut Hill, Massachusetts 02467, United States, and [‡]Institute of Chemistry, Academia Sinica, Nankang Taipei 11529, Taiwan. [§]Present address: Department of Chemistry and Chemical Biology, Harvard University, 12 Oxford Street, Cambridge, Massachusetts 02138, United States.

ABSTRACT Bimetallic nanoparticle catalysts provide enhanced activity, as combining metals allows tuning of electronic and geometric structure, but the enhancement may vary during the reaction because the nanoparticles can undergo metal migration under catalytic reaction conditions. Using cyclic voltammetry to track the surface composition over time, we carried out a detailed study of

metal migration in a well-defined model Au−Pd core−shell nanocatalyst. When subjected to electrochemical conditions, Au migration from the core to the shell was observed. The effect of Pd shell thickness and electrolyte identity on the extent of migration was studied. Migration of metals during catalytic ethanol oxidation was found to alter the particle's surface composition and electronic structure, enhancing the core−shell particles' activity. We show that metal migration in core−shell nanoparticles is a phenomenon common to numerous electrochemical systems and must be considered when studying electrochemical catalysis.
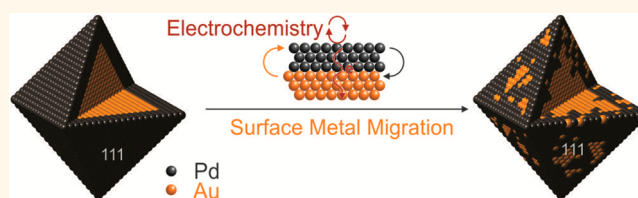
KEYWORDS: Au · Pd · metal migration · electrocatalysis · lattice strain · ethanol oxidation

Bimetallic nanoparticles (NPs) often exhibit activity superior to their monometallic counterparts, due to a combination of metal−metal interactions. Many examples of increased catalytic activity on bimetallic core−shell or alloy NPs have been published in the literature.[1−8] Electronic effects, also called ligand effects or charge redistribution, alter the electronic structure of the metal surface through direct electron interaction between the two metals. The resulting increase in activity can be explained by the position of the surface metal's d-band center in relation to the Fermi level, affecting how strongly reactive adsorbate molecules can bind to the metal surface.[9−11] The geometric effect, or lattice strain, also alters catalytic activity by changing the position of the d-band center. When two metals with different lattice sizes are brought into contact, the crystal lattice near the boundary needs to restructure a small amount to reduce the lattice mismatch. Expansive strain reduces orbital overlap, narrowing the d-band and raising the d-band center, while compressive strain increases overlap, widening the d-band and lowering the d-band center.[9,12−14] Synergy, or ensemble effects, involves the availability of specific metal active sites. Many catalytic reactions that take place on a metal surface require a specific type of binding site to achieve the correct orientation, for example, a 3-fold Pd site or a monomer Pt site, while the wrong site can lead to poisoning of the surface or unwanted byproducts. Adding a second metal to an NP catalyst can alter activity by preferentially tuning the types of active sites available to adsorbates.[15−17]
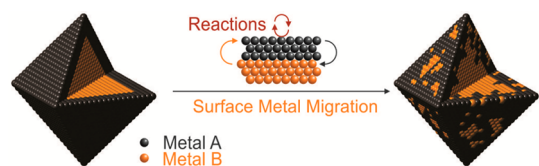
While bimetallic and multimetallic NPs often exhibit improved activity compared to their monometallic counterparts, it is

Reactions

Surface Metal Migration

● Metal A
● Metal B

Scheme 1. Surface metal migration of core−shell nanoparticles.

difficult to optimize activity by simply manipulating composition and structure, because metal migration causes the influence of electronic, geometric, and ensemble effects to change over time. Bimetallic nanoparticles undergo metal migration when subjected to reaction conditions, caused by surface energy differences and oxidizing or reducing agents in the system (Scheme 1). This has attracted great attention in recent catalysis research.[18] Using the popular core−shell structure as an example, the core metal may have lower surface energy than the shell metal, so when given enough energy, the core metal will migrate to the particle surface in order to lower the overall surface energy. Experimental and computational work has been done to study heat-induced metal migration. Computational studies modeled the high-temperature melting of Au−Pt core−shell NPs, finding the migration of Au from core to shell to be inhomogeneous and dependent on shell thickness.[19] A recent experimental study used various calcination temperatures and gas environments to migrate Au in Au−Pt core−shell NPs and manipulate the ratio of Pt to Au in the alloyed shell, finding that the migration of Au from core to shell increased catalytic activity in electro-oxidations. They attributed this result to electronic and synergetic effects: the Au in the shell both altered Pt's electronic structure and manipulated the types of active sites available.[20] It has also been found that metal migration can occur under catalytic reaction conditions. In gas phase heterogeneous catalysis, both the reaction temperature and the gases present in the reaction mixture affect metal migration. It was shown that in Rh−Pt and Rh−Pd NPs, Rh and Pd or Pt alternately and reversibly migrate to the surface as the gas environment is changed. Metallic Pd and Pt have lower surface energies than Rh, so they move to the surface under reducing conditions, but Rh forms more stable oxides, so it moves to the surface under oxidizing conditions.[21] A similar finding was achieved with Au−Pd NPs under a CO/O_2 atmosphere, in which the ratio of gases present determined the surface composition of the particles.[22] Migration has also been seen *in situ* in electrocatalytic reaction conditions, in the cases of Pt−Ni[23] and Pt−Cu.[24] In many cases, the compositional and structural changes resulting from metal migration can lead to higher activity, but may also decrease durability.

While the impact on catalysis of electrochemically induced metal migration has been shown, such study is less extensive compared to work on synthetic routes

and catalysis for metal core−shell nanoparticles. Here, we study metal migration induced by reaction conditions in a well-defined model Au−Pd core−shell nanocatalyst; a system that has been well studied synthetically.[25−28] Pd is an important catalytic metal for a number of energy- and industrially relevant reactions,[29−33] and Au has been shown to increase Pd's activity in many cases,[34,35] so this an important bimetallic system in which to study migration. Au has a lower surface energy than Pd and is prone to outward migration from core to shell.[36] The structural and compositional changes resulting from metal migration need to be studied in order to understand the stability of Au−Pd bimetallic catalysts, as well as to elucidate the real active surface of the catalyst, which may be different from that of the as-synthesized NPs. Migration in Au−Pd NPs has been studied theoretically *via* high-temperature simulations[36] and in gas phase heterogeneous catalysis,[37] but to our knowledge it has not been studied under electrocatalytic conditions. In this work, well-defined Au−Pd core−shell octahedral NPs were synthesized as a model catalyst and tested under a number of different electrochemical conditions to understand the mechanism and catalytic consequences of *in situ* metal migration. Octahedral particles were chosen because the {111} crystal facet is the most stable and close-packed low-index facet, and a 30 nm particle size was chosen because the relatively large size allows good control over shape and shell thickness. Different morphologies and sizes will be studied in the future; for an initial study, the good stability and well-controlled structure of the 30 nm octahedra provide an excellent model catalyst platform. We show that electrochemical cycling during both voltammetric profiles and catalytic ethanol oxidation induces surface composition changes, that the mechanism of change likely involves both Au migration and Pd oxidative dissolution, and that the compositional changes affect catalytic activity through a combination of bimetallic interactions.

RESULTS AND DISCUSSION

An aqueous phase, cetyltrimethylammonium bromide (CTAB)-capped synthetic method similar to that employed in our recent work[38] was used to create 30−35 nm Au−Pd core−shell nanooctahedra. As an ionic capping agent, CTAB is relatively loosely associated with the NP surface and can be removed by a combination of centrifugation in water and potential cycling, so it is a suitable capping agent with which to study surface structure and catalysis. Large, well-defined NPs with tunable shell thicknesses are suitable model catalysts for the study of metal migration, so hydrothermally synthesized Au octahedral NPs with a corner-to-corner length of 30 nm were chosen as seeds, as reported in the literature.[39] Pd was grown epitaxially over the Au seeds, and by varying the
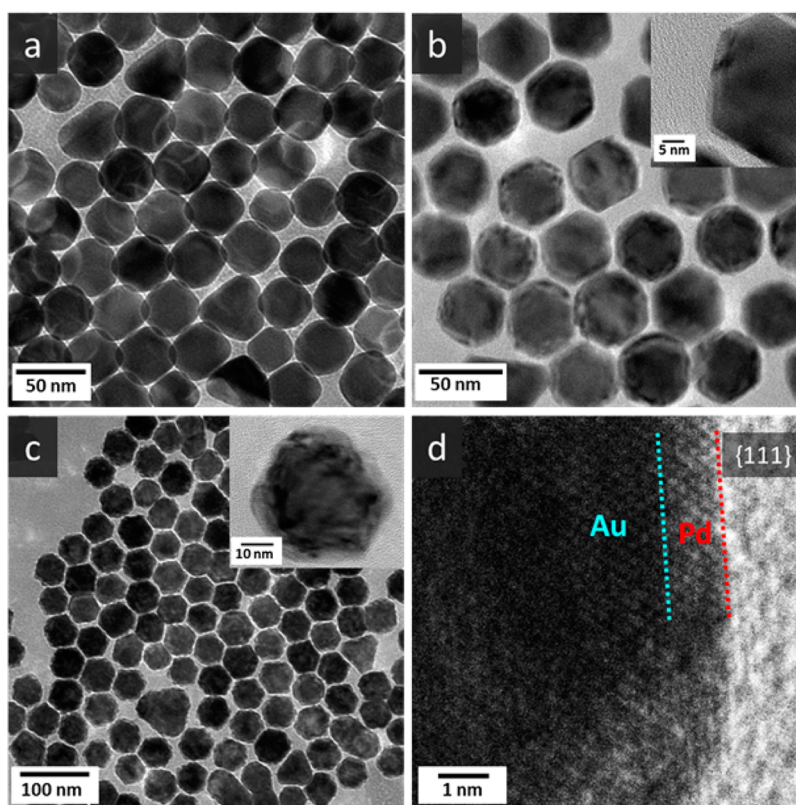
Figure 1. TEM images of (a) Au nanooctahedra, (b) thin shell Au−Pd nanooctahedra, and (c) thick shell Au−Pd nanooctahedra and (d) HR-TEM image of a thin shell octahedron's Au−Pd interface, showing epitaxial growth. Insets in (b) and (c) show magnified images of a single Au−Pd particle.

amount of Pd precursor in the growth solution, Pd shells of tunable thicknesses were obtained. Adding 15 μL of 0.01 M H_2PdCl_4 to the growth solution yielded Pd shells approximately 1.5 nm thick (thin shell), while adding 50 μL of 0.01 M H_2PdCl_4 to the growth solution yielded Pd shells approximately 4.5 nm thick (thick shell). Transmission electron microscopy (TEM) images of the Au seeds and thin and thick shell Au−Pd octahedra are shown in Figure 1. Figure 1d shows the continual lattice fringes from the Au core to Pd shell phases, indicating epitaxial growth. Both particle types have well-defined structures and good mono-dispersity, which allows us to perform the thorough electrochemical study discussed below.

Voltammetric profiles of the thin shell octahedra were performed in 0.5 M H_2SO_4 to characterize the surface composition of the particles over time. The charges associated with characteristic peaks in the profile are proportional to Au and Pd surface areas: the peaks for hydrogen adsorption and desorption on Pd (Pd−H) occur between −0.19 and 0.06 V, and the peak for oxide reduction on Au (Au-ox) occurs on the cathodic scan between 1.0 and 0.8 V.[20] Cycles 3, 10, and 20 of thin shell octahedra profiles are shown in Figure 2a. The Pd−H peaks decrease and the Au-ox peaks increase in magnitude over time, indicating increasing amounts of Au exposed on the surface. Quantitative surface areas can be obtained by averaging

the Pd−H adsorption and desorption peak charges and dividing by 212 μC/cm^2,[40] and dividing the Au-ox peak charge by 340 μC/cm^2 to give surface area in cm^2 (Figure S1).[20]

These surface areas were calculated every five cycles and are plotted against cycle number in Figure 2d. This plot shows that the Pd surface area steadily decreases while the Au surface area steadily increases. This change in surface composition could occur either by outward migration of Au from the core to the shell or by dissolution of Pd from the particle surface into the electrolyte, or by a combination of both. As a control experiment, a mixture of pure Au and Pd NPs was synthesized and tested under the same voltammetric profile conditions, shown in Figure 2b,e. After 20 cycles, little change in the shape or magnitude of the Pd−H and Au-ox peaks can be seen, and accordingly, the plot of surface area *versus* cycle number shows little change over time. The Pd surface area actually increases slightly at first, likely due to the surface becoming cleaner: while centrifugation removes excess solution CTAB, some CTAB molecules still remain associated with the surface after centrifugation,[41] and this portion is stripped away by potential cycling. This CTAB-cleaning effect is likely also present in the case of the thin shell octahedra, but the Au migration is so rapid in this case that it dwarfs the cleaning effect and Pd surface area immediately decreases. In addition,
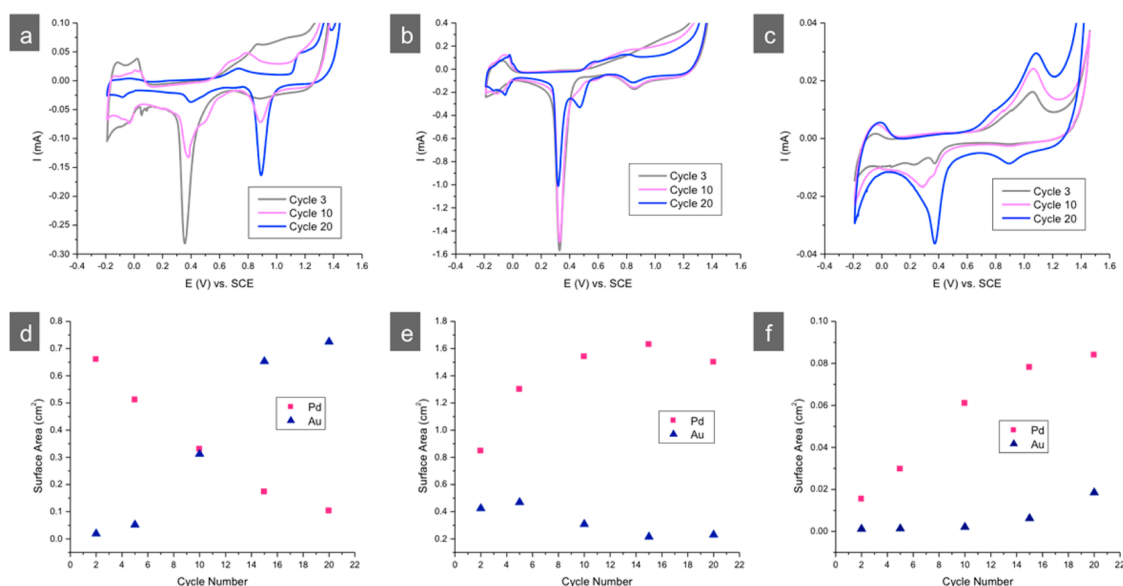
Figure 2. Voltammetric profiles of NPs in 0.5 M H_2SO_4 of (a) thin shell Au−Pd core−shell octahedra, (b) a mixture of pure Pd and Au NPs, and (c) thick shell Au−Pd core−shell octahedra. (d−f) Plots of Pd and Au surface areas calculated from voltammetric profile charges *versus* cycle number for thin shell Au−Pd core−shell octahedra, the Pd/Au mixture, and thick shell Au−Pd core−shell octahedra, respectively.

the same test was performed on the thick shell octahedra, shown in Figure 2c,f. The results are more similar to that of the Au/Pd mix than that of the thin shell octahedra: the Pd area increases slightly over the span of 20 cycles, likely due to surface cleaning. The near-steady Pd areas in Figure 2e,f indicate that Pd dissolves relatively slowly into solution under these conditions; it takes 15 cycles to initiate a slow surface area decrease of pure Pd NPs, as compared with the immediate Pd surface area decrease in the case of the thin Pd shell, which provides evidence that the observed thin shell surface changes are not solely caused by Pd dissolution. The outward migration of the Au core atoms plays a more important role here. The rapid decrease in Pd surface area observed in Figure 2d could be due to Au atoms overtaking the surface, or that Au migration destabilizes Pd surface atoms and thus initiates Pd dissolution. The Pd shell must be thin to facilitate these changes; in Figure 2c,f the Pd shell is too thick to allow Au to migrate to the surface and/or cause Pd to dissolve.

The evolution in shape and peak placement of the voltammetric profiles in Figure 2 provides more information about the structural changes occurring during the electrochemical cycling. The {100} and {111} facet dominant surfaces of Pd NPs have unique peak potentials, as the two facets adsorb hydrogen and form oxides at different energies.[42] In the hydrogen adsorption/desorption region (−0.19 to 0 V), {100} facets exhibit peaks to the right of {111}; in the oxidized Pd formation region (0.6 to 0.9 V anodic), {100} facets exhibit peaks to the left of {111}; and in the reduction of the oxidized Pd region (0.2 to 0.6 V cathodic), {100} facets exhibit peaks to the right of {111}.

It can be seen in Figure 2a,b that with increased cycling a new peak grows in at 0.5 V on the cathodic scan. This peak corresponds to the reduction of oxidized Pd on a {100} facet and grows in next to the peak at 0.35 V corresponding to the reduction of oxidized Pd on a {111} facet. In addition, the Pd−H region peaks shift to the right with increased cycling, and the oxidized Pd formation peaks shift to the left. Each of these changes indicates that the fraction of exposed {111} facets decreases while the fraction of exposed {100} facets increases. This structural change makes sense when considering Pd dissolution under these electrochemical conditions. In an octahedral NP, the corners are the most undercoordinated, and thus of highest energy, and are likely to change more easily than the more stable {111} faces, creating truncated cuboctahedral morphologies. The change of corners exposes {100} facets and gives rise to the above-mentioned {100} characteristic CV peaks. These changes in peak placement are seen to a lesser extent, however, in the case of thick shell octahedra in Figure 2c, corroborating the results of surface area measurements in Figure 2d,e,f that the lowest amount of Pd dissolution is seen in the case of the thick shell octahedra.

It is likely that the migration of Au from core to shell results from differences in surface and cohesive energies. Pd has a larger cohesive energy than Au; it is more favorable for Pd to be highly coordinated in the volume of a solid rather than undercoordinated on the edge, and this effect is stronger for Pd than for Au. In addition, Au has a lower surface energy than Pd, which combined with the cohesive energy effect is a strong driving force for Au atoms to diffuse preferentially to the NP surface and displace Pd atoms.[22] In one study,
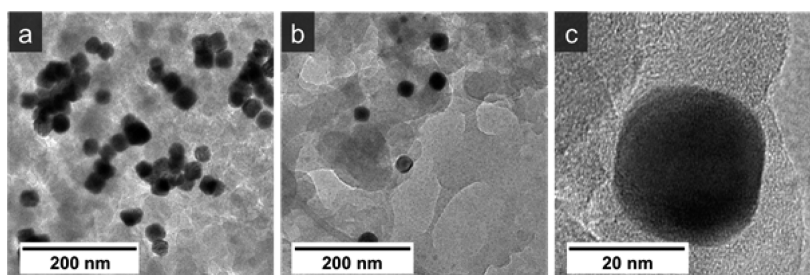
Figure 3. TEM images of thin shell Au−Pd core−shell octahedra on a Vulcan XC-72 support (a) before and (b, c) after 20 voltammetric profile cycles in 0.5 M H₂SO₄.

this energetic effect was found to induce irreversible Au migration only in Au−Pd NPs with a sufficiently thin shell, which correlates with the results in this work.[43] In a gas phase environment, the metal with lower surface energy tends to migrate outward under reducing conditions, while the more easily oxidized metal migrates outward under oxidative conditions.[21] In an electrochemical environment, the condition switches from oxidative to reducing between every scan, but the same principles may apply; on the cathodic scans the lower surface energy Au migrates outward, and on the anodic scans Pd would be expected to oxidize and migrate outward. However, it has been found that the alloying of Au with Pd reduces the number of unoccupied electronic states in Pd's d-band, inhibiting Pd oxidation.[43,44] It is possible that as Au migrates outward and the NP shell becomes alloyed, Pd can resist oxidation on the anodic scans and Au is able to remain on the surface.

TEM images were taken of the thin shell Au−Pd octahedra before and after 20 voltammetric profile cycles in 0.5 M H₂SO₄, shown in Figure 3. In order to have a tangible amount of material to collect off of the electrode after cycling, it was necessary to load the NPs onto a conductive carbon Vulcan XC-72 support before deposition onto the electrode. Figure 3b,c shows that the octahedral shape of the NPs is largely maintained during cycling, although there may be some rounding of the corners into a cuboctahedral shape due to dissolution at the corners as discussed above, and Figure 3c may indicate the retention of a core−shell structure. TEM provides little contrast between Au and Pd atoms, however, so the existence of a core−shell structure or alloyed shell cannot be determined conclusively, and due to varied orientation on the three-dimensional carbon support, it is difficult to ascertain the exact NP shape.

Scanning transmission electron microscopy (STEM) equipped with energy-dispersive X-ray spectroscopy (EDX) was used to study the Au−Pd thin shell core−shell octahedra before and after 20 cycles of voltammetric profile scanning in 0.5 M H₂SO₄. The resulting line scans are shown in Figure 4, along with crystal models depicting what we believe to be the Au−Pd structures before and after voltammetric profile scanning.

The Pd line scan (red) before cycling has a sharp peak at each end, indicative of a well-defined core−shell structure; the as-synthesized octahedra have a clear boundary between the Au core and Pd shell. The Pd line scan after cycling, on the other hand, lacks this characteristic feature and rather has a smooth bell curve shape similar to that of Au (blue), indicating the presence of both metals in the shell due to Au migration. The presence of both Au and Pd in the particle shell is corroborated by the presence of both Au and Pd peaks in the voltammetric profiles. STEM elemental mapping was also obtained of the Au−Pd octahedra, shown in Supporting Information Figure S2. The before and after maps appear similar, but it is important to note that even after cycling there remains virtually no Pd in the interior of the particle. This indicates that while Au migrates to the shell, there is little to no migration of Pd toward the core. Therefore, one possible mechanism of compositional change is that Au atoms migrate to the shell and displace Pd atoms, which then dissolve into solution instead of dissolving back into the interior of the NP. Or, Pd atoms first dissolve from the shell surface into solution, and Au atoms migrate into the shell to fill the vacancies left behind. The latter may be more likely, because when Pd atoms dissolve out of the shell, they leave high-energy, undercoordinated sites and it becomes energetically favorable for Au atoms to fill these sites. The results of voltammetric profiles and surface area quantification (Figure 1) indicate that Pd does not dissolve into the solution on its own, as little decrease in Pd area was seen for pure Pd particles or a thick Pd shell. This implies that some modification or influence by the Au core may be needed to induce Pd dissolution and that the processes of Au migration and Pd dissolution are closely related.

Next, the effect of electrolyte on Au migration was studied by comparing voltammetric profiles of thin shell Au−Pd octahedra in 0.5 M sulfuric acid, perchloric acid, and potassium hydroxide, shown in Figure 5. These three electrolytes are the most commonly used in electrochemical NP characterization and were thus tested in order to gain a general understanding of metal migration behavior in voltammetric profiles, in both acidic and alkaline solutions. In sulfuric acid, a drastic change in Pd−H and Au-ox peaks can be seen
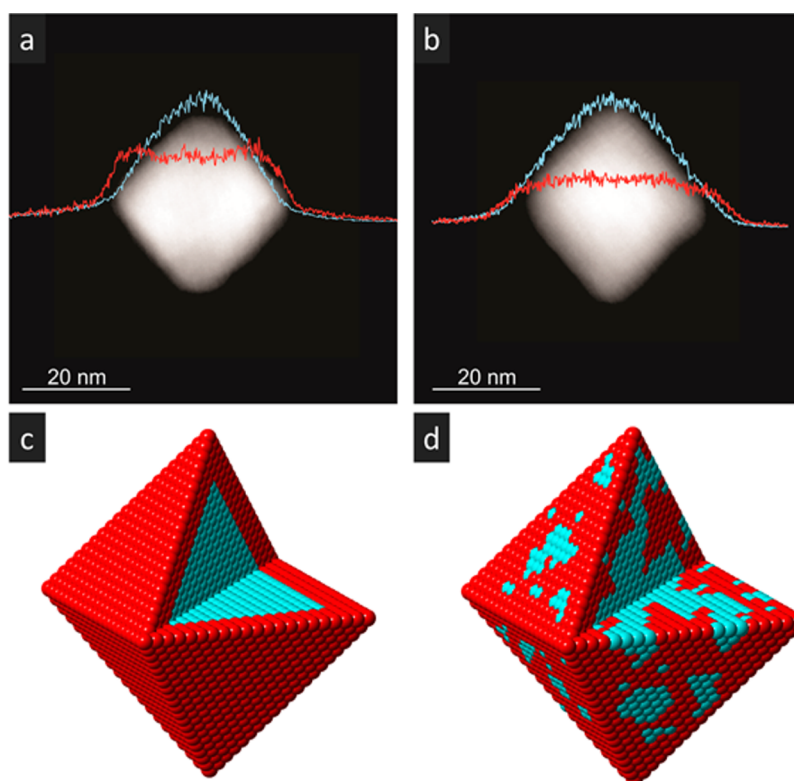
Figure 4. EDX line scans of Au−Pd thin shell core−shell octahedra on a Vulcan XC-72 support (a) as synthesized and (b) after 20 voltammetric profile cycles in 0.5 M H$_2$SO$_4$. (c, d) Crystal models of what we believe the NPs look like before cycling (core−shell) and after cycling (core−alloyed-shell). Pd is shown in red; Au in blue.
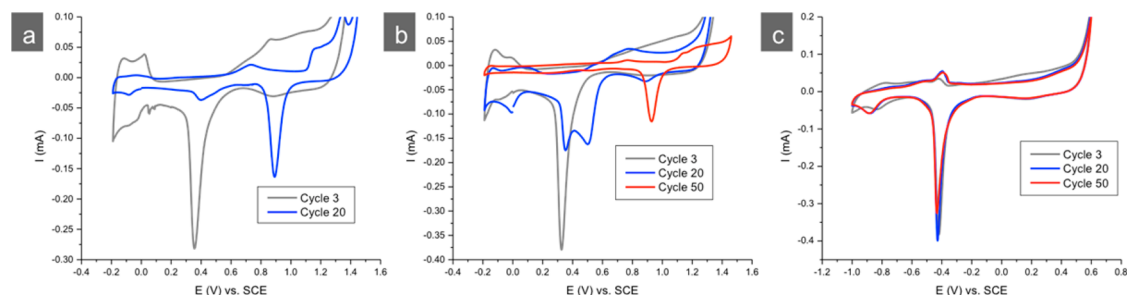

Figure 5. Voltammetric profiles of thin shell Au−Pd core−shell octahedra in (a) 0.5 M H$_2$SO$_4$, (b) 0.5 M HClO$_4$, and (c) 0.5 M KOH. A drastic change in surface composition is seen in H$_2$SO$_4$, while less change is seen in HClO$_4$ and no change is seen in KOH.

between cycles 3 and 20; by cycle 20 the Pd−H peaks have diminished to almost nothing and the Au-ox peak has grown large. In perchloric acid, on the other hand, the Pd−H and Au-ox peaks in cycles 3 and 20 differ minimally, and a drastic change as seen in sulfuric acid is not seen until cycle 50. In KOH, no change is seen even after 50 cycles. A different voltage range is needed for the KOH scans, but it has been shown that the characteristic peaks fall in the same relative positions;[45] thus the lack of change in the Pd−H and Au-ox peaks still indicates little to no migration/dissolution. In addition, the changes in peak placement with repeated cycling discussed above are seen in Figure 5a,b but not c, again indicating little to no Pd dissolution in the KOH electrolyte. These results

indicate that Au is able to migrate the fastest, and/or Pd dissolves the fastest, in sulfuric acid, slowly in perchloric acid, and not at all in an alkaline environment. The difference in migration/dissolution between acid electrolytes likely results from the different anions in solution. It has been reported that Pd's anodic oxidation and dissolution occurs to a different extent depending on the electrolyte.[46] The presence of anions in solution may facilitate the formation of dissolution intermediates or products by forming complexes with Pd cations, so the anion identity can affect the rate of dissolution. ClO$_4^-$ anions are known to promote Pd dissolution to a lesser extent,[47] and to adsorb to Pd surfaces to a lesser extent,[48] than HSO$_4^-$/SO$_4^{2-}$. Thus, the HClO$_4$ electrolyte interacts less with the Pd

surface and does not induce migration/dissolution as fast as H_2SO_4.

As noted above, the potential range for the KOH profiles is different than that of the acidic electrolytes, only scanning to 0.6 V, so it is possible that a higher anodic potential is needed to induce Au migration and Pd dissolution, resulting in no compositional change in the KOH profile. We also note that there is no sulfate anion present in the KOH experiment, so the anion effect may also be at play in this system; OH^- anions may not facilitate Pd dissolution to the same extent as ClO_4^- and HSO_4^-/SO_4^{2-}. To further study the effect of pH on metal migration, voltammetric profiles of thin shell Au−Pd octahedra were obtained in pH 4, 7, and 10 0.5 M SO_4^{2-} electrolyte solutions, shown in Figure S3. Migration is observed in the pH 4 profile, as evidenced by the disappearance of the Pd−H peaks and the appearance of the Au-ox peak, while little to no migration is observed in the profiles at pH 7 and 10. In addition, the migration at pH 4 is observed to a lesser extent than that at pH 0 (0.5 M H_2SO_4 in Figure 5a). Because the characteristic Pd−H and Au-ox peaks occur at different potentials depending on the electrolyte pH, slightly different potential windows were necessary for each experiment (pH 0: −0.19 to 1.49 V, pH 4: −0.5 to 1.26 V, pH 7 and 10: −1.0 to 1.2 V). However, the anodic potentials are sufficiently high in each case to fully oxidize both Pd and Au, so the trend observed is due to differences in pH rather than potential. It is known that Pd dissolution occurs to a greater extent at lower pH,[47] and it is likely that a sufficiently acidic electrolyte is necessary in this system to induce Pd dissolution and Au migration. To limit unwanted metal migration in bimetallic catalyst systems, therefore, it may be beneficial to perform reactions in an alkaline environment when possible.

Next, the migration of Au was studied under catalytic conditions. Ethanol electro-oxidation is an important fuel cell reaction and, as such, has become a popular characterization method with which to test the activity of metal nanoparticles. While it is a widely utilized reaction, the effect of metal migration on ethanol oxidation activity in such a well-defined system is unstudied, making it a perfect model reaction for this work. The ethanol oxidation reaction (EOR) in an alkaline electrolyte was performed on the thin and thick shell Au−Pd octahedral NPs to study both the effect of migration on electrocatalysis and the effect of shell thickness on migration. In order to compare activity of the two NP types, an electrochemically active surface area (ECSA) measurement with which to normalize current is needed. CO stripping is generally the best method for ECSA quantification, but did not give readable currents for these NPs. Voltammetric profiles can also be used to calculate ECSA, but as discussed above, these scans alter the NP surface. Instead, "half" blank scans, cycling from 0.19 to 0.3 V,

were performed, thus avoiding the highly anodic region that causes Au migration and/or Pd dissolution. After 20 cycles of "half" blank scans, no change was seen, indicating no surface modification (Figure S4). Pd ECSA was determined by averaging the Pd−H peaks and dividing by 212 $\mu C/cm^2$ as above. Two thousand cycles of ethanol oxidation were performed, and cycles 2, 500, and 2000 for thin and thick shell Au−Pd octahedra are shown in Figure 6. In the case of thin shell octahedra, two main peaks are present until about cycle 400, at which point two new peaks appear. These peaks are labeled I−IV in Figure 6a. Forward peak I and backward peak IV are in positions characteristic of ethanol oxidation on Pd,[49] while forward peak II and backward peak III are characteristic of ethanol oxidation on Au (Figure S5).[50] The presence of Au peaks indicates again that during electrochemical cycling Au migrates from the NP core to the shell. The normalized current densities of these peaks were measured every one hundred cycles and are plotted against cycle number in Figure 6c,d. For the thin shell octahedra, Pd's current density peaks around cycle 400, near 80 mA/cm^2, and begins to decrease steadily as Au peaks appear. The Au peaks hit a maximum at about 800 cycles before beginning to steadily decrease. The activity of all four peaks eventually flattens out near 10 mA/cm^2. The presence of Au peaks indicates migration of Au from core to shell, which interestingly does not occur until cycle 400, while occurring in the first 10 cycles in sulfuric acid voltammetric profiles. This may be due to the alkaline electrolyte or the low anodic voltage (the scans cycle from −0.8 to 0.3 V). The case of thick shell Au−Pd octahedra is strikingly different; Au peaks II and III never appear, indicating no migration of Au from core to shell, and the Pd activity reaches a maximum at cycle 100 near 14 mA/cm^2 and decreases rapidly, flattening out near 1 mA/cm^2. Thus, the thick Pd shell prevents Au migration, but the thin Pd shell provides a much higher overall current density of 80 versus 14 mA/cm^2 at peak and 10 versus 1 mA/cm^2 after 2000 cycles. It is also important to note that the thin shell octahedra increase in activity for the first 400 cycles; as Au moves toward the surface, it promotes Pd EOR activity, but when the Au surface coverage is too high, activity decreases.

These trends in activity can be explained by a combination of lattice strain, ligand, and ensemble effects. Au has a larger lattice size than Pd and expands Pd's lattice, raising its d-band center and increasing adsorbate bonding strength.[38] This effect can only be seen for sufficiently thin Pd shells and thus increases EOR activity for thin shell but not thick shell octahedra.[25,51] Ligand effects are likely also at play in this system. In general, electron density transfers from the metal with the higher Fermi level (Pd in this case) to the metal with the lower Fermi level (Au). However, in
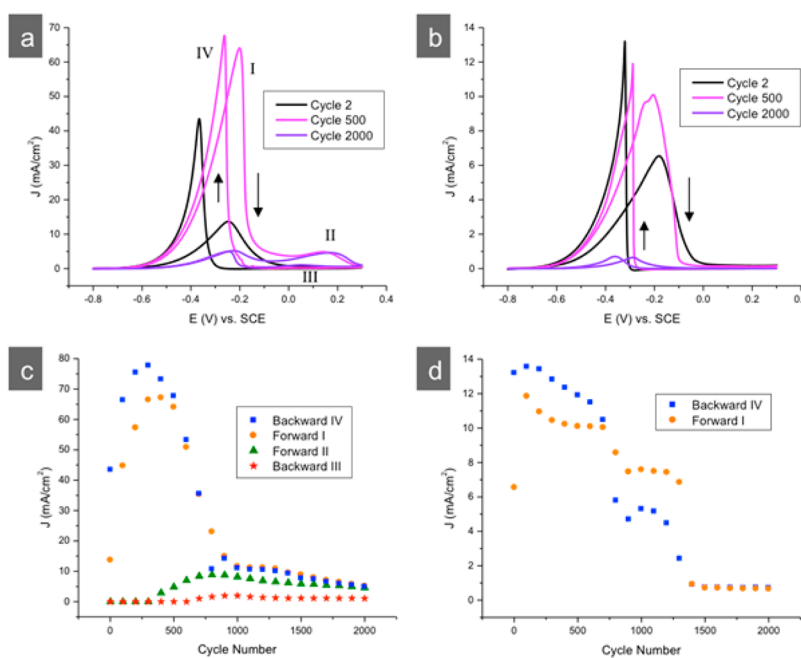
Figure 6. (a, b) Ethanol oxidation reaction (EOR) performed on thin and thick shell Au−Pd core−shell octahedra, respectively, in 1 M KOH + 1 M ethanol. (c, d) Plots of EOR current density *versus* cycle number for thin and thick shell octahedra, respectively, for peaks I−IV as labeled in (a).

the special case of AuPd alloys, the opposite occurs, and even though s and p orbital electron density is transferred from Pd to Au, the catalytically important d orbital electron density is transferred from Au to Pd, lowering Pd's d-band center and decreasing the bonding strength of adsorbates.[52] Thus, strain and ligand effects work in opposition here. In the thin shell core−shell system, ligand effects are not yet present, and strain effects promote EOR activity by increasing chemisorption of ethanol. It is likely that in the first 400 cycles Au moves closer toward the shell and strain effects increase, hence the increase in EOR activity. After 400 cycles, however, Au is exposed on the surface—as evidenced by the appearance of peaks II and III—and the surface becomes a AuPd alloy. Once the alloy is present, ligand effects play a more important role and begin to weaken ethanol chemisorption, decreasing EOR activity. One study notes that the AuPd alloy ligand effect is not seen in Pd monolayers or thick shells, but requires Pd monomers surrounded by Au atoms,[52] and becomes present once Au migrates to the shell in this case. In addition, as Au displaces surface Pd atoms, the number of ensemble Pd active sites on which ethanol oxidation takes place decreases, contributing along with ligand effects to the decrease in Pd EOR activity. In the thick shell octahedra, on the other hand, neither strain nor ligand nor ensemble effects are present, and the Pd shell acts much like a pure Pd catalyst. There is no Au-induced lattice expansion to promote activity and activity remains low. Activity decreases with repeated cycling, possibly due to poisoning or oxidation of the Pd surface, which is not protected by Au alloying as in the thin shell case.[43,44]

CONCLUSION

In this study, Au−Pd core−shell octahedral NPs with tunable thicknesses were synthesized and tested electrochemically. It was found that under electrochemical conditions Au migrates outward from the core to the shell, and the extent of migration depends on the identity and pH of the electrolyte, as well as the potential range used. STEM/EDX imaging and mapping of the octahedra post-electrochemical cycling and voltammetric profiles of an Au/Pd mixture provide evidence for the compositional and structural changes occurring by a combination of both Au migration and Pd dissolution mechanisms. Lastly, thin and thick shell Au−Pd core−shell octahedra were compared as EOR catalysts. It was found that migration was more prevalent in the thin shell particles, at first promoting EOR activity by strain effects but then inhibiting activity by ligand and ensemble effects. The thick octahedral shell prevented migration but also inhibited Au-induced strain effects, resulting in overall low catalytic activity. These results are interesting and instructive: in many reported bimetallic NP studies, scientists have focused on the activity of the first few electrocatalytic cycles, which has contributed a great understanding of ligand, strain, and ensemble effects. Yet, this study shows that structure and composition, and therefore activity, change over time during electrocatalysis. In addition, these results indicate that metal migration could be used to our advantage, by subjecting particles to electrochemical conditions to achieve a specific amount of migration, before using the particles as catalysts. Ligand, strain, and ensemble effects play different roles in tuning catalytic

activity at different stages of migration; thus, by selecting a number of electrochemical cycles we could manipulate migration to optimize these bimetallic effects and achieve enhanced catalytic activity.

METHODS

Chemicals. L-Ascorbic acid (99%), hydrochloric acid (HCl, 37%), palladium(II) chloride (PdCl$_2$, 99%), gold(III) chloride trihydrate (AuCl$_3$·3H$_2$O, ~50% Au by wt), sodium citrate tribasic dihydrate (Na$_3$C$_6$H$_5$O$_7$·2H$_2$O, 99.5%), and perchloric acid (HClO$_4$, 70%) were all obtained from Sigma-Aldrich. Cetyltrimethylammonium bromide (98%) was obtained from Calbiochem. Cetyltrimethylammonium chloride (99%) was obtained from Fluka. Sulfuric acid (H$_2$SO$_4$, 95%) and sodium hydroxide (NaOH, 95%) were obtained from BDH. Nitrogen gas (99%) was obtained from Airgas. Ethanol (CH$_3$OH, 99.8%) was obtained from Acros. Deionized water (18.2 MΩ) was used in all procedures. Hydrochloric acid was used to prepare the acidic precursors for gold and palladium. Concentrated HCl was diluted, added to a beaker containing the metal chloride salt, and stirred under gentle heating to produce the 0.01 M stock solutions.

Synthesis of 30 nm Au Nanooctahedra. First, deionized water (97 mL) was added to a glass hydrothermal vessel that contained CTAB (550 mg), and sonication was applied to dissolve the CTAB. Next, a 0.01 M solution of HAuCl$_4$ (2.500 mL) was added, along with a 0.1 M solution of sodium citrate (0.500 mL). The hydrothermal vessel was placed in an oven at 110 °C for 24 h. The final solution was centrifuged at 6000 rpm for 20 min. This process was repeated two more times to ensure that any excess surfactant was removed. Lastly, the resulting clear supernatant was discarded, and the particles were redispersed in water (10 mL).

Synthesis of 35 nm Au–Pd Core–Shell Nanooctahedra. First, deionized water (10 mL) was added to a 20 mL vial containing CTAB (50 mg), and sonication was applied to dissolve the CTAB. Then, a portion of 30 nm Au octahedral seeds (0.500 mL) was added to the solution. Next, a portion of 0.01 M solution of H$_2$PdCl$_4$ (15 or 50 μL) was added, along with a 0.04 M solution of ascorbic acid (0.100 mL). A stir bar was added, and the capped vial was placed in a water bath at 40 °C for 24 h with gentle stirring. These particles were washed by centrifugation at 6000 rpm for 10 min. This process was repeated two more times. The final clear supernatant was discarded, and the particles were redispersed in water (1 mL). Synthesis with 15 μL of 0.01 M H$_2$PdCl$_4$ gave core–shell nanooctahedra with a ~1.5 nm shell, while synthesis with 50 μL of 0.01 M H$_2$PdCl$_4$ gave core–shell nanooctahedra with a ~4.5 nm shell.

Characterization. Samples were prepared for TEM by washing several times with DI water and placing 1.0 μL droplets of particle solutions on carbon-coated copper grids, which were then allowed to dry in air. The instrument used for TEM was a JEOL JEM2010F operated at 200 kV. High-resolution STEM and EDX mapping experiments were performed on a FEI Probe Cs corrected Titan operating at 200 kV. The high-angle annular dark field (HAADF) images were acquired by a Fischione HAADF detector, and the EDX maps were acquired by ChemiSTEM technology with four windowless SDD detectors. This instrument incorporates the condenser spherical aberration corrector and X-FEG with probe current 0.4 nA in a 0.31 nm spot and can achieve a resolution of 0.08 nm as well as efficient X-ray collection rate.

Electrochemical Measurements. A concentrated particle solution (5 μL) was deposited onto the previously alumina-polished surface of a glassy carbon working electrode (CH Instruments). A typical three-electrode system was used to perform the electrochemical experiments: a glassy carbon working electrode with deposited particles, a saturated calomel electrode (SCE) reference electrode, and a platinum auxiliary electrode (both CH Instruments) were connected to a potentiostat system (BioLogic VSP). The electrodes were put into a three-neck flask containing aqueous electrolyte solutions that had been previously bubbled with nitrogen gas. Voltammetric profiles were carried out in 0.5 M H$_2$SO$_4$ scanning from −0.19 to 1.46 V at 50 mV/s; in 0.5 M HClO$_4$ from −0.19 to 1.46 V at 50 mV/s; and in 0.5 M KOH from −1.0 to 0.6 V at 50 mV/s. Ethanol oxidation was performed in a 1 M KOH + 1 M ethanol solution, scanning from −0.8 to 0.3 V at a scan rate of 50 mV/s. The current was normalized by Pd area, determined by measuring the hydrogen adsorption/desorption charge in a sulfuric acid blank scan.

Conflict of Interest: The authors declare no competing financial interest.

REFERENCES AND NOTES

1. Tedsree, K.; Li, T.; Jones, S.; Chan, C. W. A.; Yu, K. M. K.; Bagot, P. A. J.; Marquis, E. A.; Smith, G. D. W.; Tsang, S. C. E. Hydrogen Production from Formic Acid Decomposition at Room Temperature Using a Ag-Pd Core-Shell Nanocatalyst. *Nat. Nanotechnol.* **2011**, *6*, 302–307.
2. Deng, Y.-J.; Tian, N.; Zhou, Z.-Y.; Huang, R.; Liu, Z.-L.; Xiao, J.; Sun, S.-G. Alloy Tetrahexahedral Pd-Pt Catalysts: Enhancing Significantly the Catalytic Activity by Synergy Effect of High-Index Facets and Electronic Structure. *Chem. Sci.* **2012**, *3*, 1157–1161.
3. Hong, J.; Kang, S.; Choi, B.; Kim, D.; Lee, S.; Han, S. Controlled Synthesis of Pd-Pt Alloy Hollow Nanostructures with Enhanced Catalytic Activities for Oxygen Reduction. *ACS Nano* **2012**, *6*, 2410–2419.
4. Taufany, F.; Pan, C.; Rick, J.; Chou, H.; Tsai, M.; Hwang, B.; Liu, D.; Lee, J.; Tang, M.; Lee, Y.; *et al.* Kinetically Controlled Autocatalytic Chemical Process for Bulk Production of Bimetallic Core-Shell Structured Nanoparticles. *ACS Nano* **2011**, *5*, 9370–9381.
5. Tsiakaras, P. PtM/C (M = Sn, Ru, Pd, W) Based Anode Direct Ethanol-PEMFCs: Structural Characteristics and Cell Performance. *J. Power Sources* **2007**, *171*, 107–112.
6. Xiao, C. X.; Wang, L. L.; Maligal-Ganesh, R. V.; Smetana, V.; Walen, H.; Thiel, P. A.; Miller, G. J.; Johnson, D. D.; Huang, W. Y. Intermetallic NaAu$_2$ as a Heterogeneous Catalyst for Low-Temperature CO Oxidation. *J. Am. Chem. Soc.* **2013**, *135*, 9592–9595.
7. Li, Q.; Jiang, R. B.; Ming, T.; Fang, C. H.; Wang, J. F. Crystalline Structure-Dependent Growth of Bimetallic Nanostructures. *Nanoscale* **2012**, *4*, 7070–7077.
8. Zhu, Y.; Zhang, S. R.; Ye, Y. C.; Zhang, X. Q.; Wang, L.; Zhu, W.; Cheng, F.; Tao, F. Catalytic Conversion of Carbon Dioxide to Methane on Ruthenium-Cobalt Bimetallic Nanocatalysts and Correlation between Surface Chemistry of Catalysts under Reaction Conditions and Catalytic Performances. *ACS Catal.* **2012**, *2*, 2403–2408.
9. Kitchin, J.; Norskov, J.; Barteau, M.; Chen, J. Role of Strain and Ligand Effects in the Modification of the Electronic and Chemical Properties of Bimetallic Surfaces. *Phys. Rev. Lett.* **2004**, *93*, 156801–156804.
10. Tang, W.; Henkelman, G. Charge Rdistribution in Core-Shell Nanoparticles to Promote Oxygen Reduction. *J. Chem. Phys.* **2009**, *130*, 194504–194504.
11. Hu, S.; Scudiero, L.; Ha, S. Electronic Effect on Oxidation of Formic Acid on Supported Pd-Cu Bimetallic Surface. *Electrochim. Acta* **2012**, *83*, 354–358.
12. Mavrikakis, M.; Hammer, B.; Norskov, J. K. Effect of Strain on the Reactivity of Metal Surfaces. *Phys. Rev. Lett.* **1998**, *81*, 2819–2822.

13. Kibler, L.; El-Aziz, A.; Hoyer, R.; Kolb, D. Tuning Reaction Rates by Lateral Strain in a Palladium Monolayer. *Angew. Chem., Int. Ed.* **2005**, *44*, 2080–2084.

14. Wang, X.; Orikasa, Y.; Takesue, Y.; Inoue, H.; Nakamura, M.; Minato, T.; Hoshi, N.; Uchimoto, Y. Quantitating the Lattice Strain Dependence of Monolayer Pt Shell Activity toward Oxygen Reduction. *J. Am. Chem. Soc.* **2013**, *135*, 5938–5941.

15. Burda, C.; Chen, X. B.; Narayanan, R.; El-Sayed, M. A. Chemistry and Properties of Nanocrystals of Different Shapes. *Chem. Rev.* **2005**, *105*, 1025–1102.

16. Cui, C.; Li, H.; Cong, H.; Yu, S.; Tao, F. Direct Evidence for Active Site-Dependent Formic Acid Electro-Oxidation by Topmost-Surface Atomic Redistribution in a Ternary PtPdCu Electrocatalyst. *Chem. Chem.* **2012**, *48*, 12062–12064.

17. Wang, X.; Wang, M.; Zhou, D.; Xia, Y. Structural Design and Facile Synthesis of a Highly Efficient Catalyst for Formic Acid Electrooxidation. *Phys. Chem. Chem. Phys.* **2011**, *13*, 13594–13597.

18. Tao, F.; Grass, M. E.; Zhang, Y.; Butcher, D. R.; Renzas, J. R.; Liu, Z.; Chung, J. Y.; Mun, B. S.; Salmeron, M.; Somorjai, G. A. Reaction-Driven Restructuring of Rh-Pd and Pt-Pd Core-Shell Nanoparticles. *Science* **2008**, *322*, 932–934.

19. Huang, R.; Wen, Y.-H.; Shao, G.-F.; Sun, S.-G. Insight into the Melting Behavior of Au-Pt Core-Shell Nanoparticles from Atomistic Simulations. *J. Phys. Chem. C* **2013**, *117*, 4278–4286.

20. Suntivich, J.; Xu, Z.; Carlton, C. E.; Kim, J.; Han, B.; Lee, S. W.; Bonnet, N.; Marzari, N.; Allard, L. F.; Gasteiger, H. A.; *et al*. Surface Composition Tuning of Au-Pt Bimetallic Nanoparticles for Enhanced Carbon Monoxide and Methanol Electro-oxidation. *J. Am. Chem. Soc.* **2013**, *135*, 7985–7991.

21. Tao, F.; Grass, M. E.; Zhang, Y.; Butcher, D. R.; Aksoy, F.; Aloni, S.; Altoe, V.; Alayoglu, S.; Renzas, J. R.; Tsung, C.-K.; *et al*. Evolution of Structure and Chemistry of Bimetallic Nanoparticle Catalysts under Reaction Conditions. *J. Am. Chem. Soc.* **2010**, *132*, 8697–8703.

22. Alayoglu, S.; Tao, F.; Altoe, V.; Specht, C.; Zhu, Z.; Aksoy, F.; Butcher, D. R.; Renzas, R. J.; Liu, Z.; Somorjai, G. A. Surface Composition and Catalytic Evolution of Au (x) Pd1-x (x=0.25, 0.50 and 0.75) Nanoparticles under CO/O₂ Reaction in Torr Pressure Regime and at 200 °C. *Catal. Lett.* **2011**, *141*, 633–640.

23. Tuaev, X.; Rudi, S.; Petkov, V.; Hoell, A.; Strasser, P. *In-Situ* Study of Atomic Structure Transformations of Pt-Ni Nanoparticle Catalysts during Electrochemical Potential Cycling. *ACS Nano* **2013**, *l*, 5666–5674.

24. Mani, P.; Srivastava, R.; Strasser, P. Dealloyed Pt-Cu Core-Shell Nanoparticle Electrocatalysts for Use in PEM Fuel Cell Cathodes. *J. Phys. Chem. C* **2008**, *112*, 2770–2778.

25. Bhattarai, N.; Casillas, G.; Khanal, S.; Salazar, J.; Ponce, A.; Jose-Yacaman, M. Origin and Shape Evolution of Core-Shell Nanoparticles in Au-Pd: From Few Atoms to High Miller Index Facets. *J. Nanopart. Res.* **2013**, *15*, 1–13.

26. Lu, C.; Prasad, K.; Wu, H.; Ho, J.; Huang, M. Au Nanocube-Directed Fabrication of Au-Pd Core-Shell Nanocrystals with Tetrahexahedral, Concave Octahedral, and Octahedral Structures and Their Electrocatalytic Activity. *J. Am. Chem. Soc.* **2010**, *132*, 14546–14553.

27. Yang, C.; Chanda, K.; Lin, P.; Wang, Y.; Liao, C.; Huang, M. Fabrication of Au-Pd Core-Shell Heterostructures with Systematic Shape Evolution Using Octahedral Nanocrystal Cores and Their Catalytic Activity. *J. Am. Chem. Soc.* **2011**, *133*, 19993–20000.

28. DeSantis, C. J.; Skrabalak, S. E. Size-Controlled Synthesis of Au/Pd Octopods with High Refractive Index Sensitivity. *Langmuir* **2012**, *28*, 9055–9062.

29. Jin, M.; Liu, H.; Zhang, H.; Xie, Z.; Liu, J.; Xia, Y. Synthesis of Pd Nanocrystals Enclosed by {100} Facets and with Sizes < 10 nm for Application in CO Oxidation. *Nano Res.* **2011**, *4*, 83–91.

30. Tedsree, K.; Li, T.; Jones, S.; Chan, C.; Yu, K.; Bagot, P.; Marquis, E.; Smith, G.; Tsang, S. Hydrogen Production from Formic Acid Decomposition at Room Temperature Using a Ag-Pd Core-Shell Nanocatalyst. *Nat. Nanotechnol.* **2011**, *6*, 302–307.

31. Meng, H.; Wang, C.; Shen, P.; Wu, G. Palladium Thorn Clusters as Catalysts for Electrooxidation of Formic Acid. *Energy Environ. Sci.* **2011**, *4*, 1522–1526.

32. Hokenek, S.; Kuhn, J. N. Methanol Decomposition over Palladium Particles Supported on Silica: Role of Particle Size and Co-Feeding Carbon Dioxide on the Catalytic Properties. *ACS Catal.* **2012**, *2*, 1013–1019.

33. Jin, T.; Guo, S. J.; Zuo, J. L.; Sun, S. H. Synthesis and Assembly of Pd Nanoparticles on Graphene for Enhanced Electrooxidation of Formic Acid. *Nanoscale* **2013**, *5*, 160–163.

34. Feng, Y.; Liu, Z.; Xu, Y.; Wang, P.; Wang, W.; Kong, D. Highly Active PdAu Alloy Catalysts for Ethanol Electro-Oxidation. *J. Power Sources* **2013**, *232*, 99–105.

35. Srejic, I.; Smiljanic, M.; Grgur, B.; Rakocevic, Z.; Strbac, S. Catalysis of Oxygen Reduction on Au Modified by Pd Nanoislands in Perchloric Acid Solution. *Electrochim. Acta* **2012**, *64*, 140–146.

36. Huang, R.; Wen, Y.; Shao, G.; Zhu, Z.; Sun, S. Thermal Stability and Shape Evolution of Tetrahexahedral Au-Pd Core-Shell Nanoparticles with High-Index Facets. *J. Phys. Chem. C* **2013**, *117*, 6896–6903.

37. Delannoy, L.; Giorgio, S.; Mattei, J.; Henry, C.; El Kolli, N.; Methivier, C.; Louis, C. Surface Segregation of Pd from TiO₂-Supported AuPd Nanoalloys under CO Oxidation Conditions Observed *in-Situ* by ETEM and DRIFTS. *ChemCatChem* **2013**, *5*, 2707–2716.

38. Kuo, C.-H.; Lamontagne, L. K.; Brodsky, C. N.; Chou, L.-Y.; Zhuang, J.; Sneed, B. T.; Sheehan, M. K.; Tsung, C.-K. The Effect of Lattice Strain on the Catalytic Properties of Pd Nanocrystals. *ChemSusChem* **2013**, *6*, 1993–2000.

39. Chang, C.; Wu, H.; Kuo, C.; Huang, M. Hydrothermal Synthesis of Monodispersed Octahedral Gold Nanocrystals with Five Different Size Ranges and Their Self-Assembled Structures. *Chem. Mater.* **2008**, *20*, 7570–7574.

40. Jukk, K.; Alexeyeva, N.; Johans, C.; Kontturi, K.; Tammeveski, K. Oxygen Reduction on Pd Nanoparticle/Multi-Walled Carbon Nanotube Composites. *J. Electroanal. Chem.* **2012**, *666*, 67–75.

41. Sau, T. K.; Murphy, C. J. Self-Assembly Patterns Formed Upon Solvent Evaporation of Aqueous Cetyltrimethylammonium Bromide-Coated Gold Nanoparticles of Various Shapes. *Langmuir* **2005**, *21*, 2923–2929.

42. Zalineeva, A.; Coutanceau, C.; Jerkiewicz, G. Electrochemical Behavior of Unsupported Shaped Palladium Nanoparticles. *Langmuir* **2014**, 10.1021/la5025229.

43. Wilson, A.; Sun, K.; Chi, M.; White, R.; LeBeau, J.; Lamb, H.; Wiley, B. From Core-Shell to Alloys: The Preparation and Characterization of Solution-Synthesized AuPd Nanoparticle Catalysts. *J. Phys. Chem. C* **2013**, *117*, 17557–17566.

44. Sasaki, K.; Naohara, H.; Choi, Y.; Cai, Y.; Chen, W.; Liu, P.; Adzic, R. Highly Stable Pt Monolayer on PdAu Nanoparticle Electrocatalysts for the Oxygen Reduction Reaction. *Nat. Commun.* **2012**, *3*, 2–9.

45. Tripkovic, A.; Popovic, K.; Grgur, B.; Blizanac, B.; Ross, P.; Markovic, N. Methanol Electrooxidation on Supported Pt and PtRu Catalysts in Acid and Alkaline Solutions. *Electrochim. Acta* **2002**, *47*, 3707–3714.

46. Harrison, J.; Whitfield, T. The Dissolution of Palladium in Various Electrolytes. *Electrochim. Acta* **1983**, *28*, 1229–1236.

47. Grden, M.; Lukaszewski, M.; Jerkiewicz, G.; Czerwinski, A. Electrochemical Behavior of Palladium Electrode: Oxidation, Electrodissolution, and Ionic Adsorption. *Electrochem. Acta* **2008**, *53*, 7583–7598.

48. Bolzan, A. E.; Arvia, A. J. Effect of the Electrolyte Composition on the Electroreduction of Palladium Oxide Films. *J. Electroanal. Chem.* **1993**, *354*, 243–253.

49. Zhou, Z.; Wang, Q.; Lin, J.; Tian, N.; Sun, S. *In-Situ* FTIR Spectroscopic Studies of Electrooxidation of Ethanol on Pd Electrode in Alkaline Media. *Electrochim. Acta* **2010**, *55*, 7995–7999.

50. Cherevko, S.; Kulyk, N.; Chung, C. Utilization of Surface Active Sites on Gold in Preparation of Highly Reactive

Interfaces for Alcohols Electrooxidation in Alkaline Media. *Electrochim. Acta* **2012**, *69*, 190–196.

51. Ding, Y.; Fan, F.; Tian, Z.; Wang, Z. Atomic Structure of Au-Pd Bimetallic Alloyed Nanoparticles. *J. Am. Chem. Soc.* **2010**, *132*, 12480–12486.

52. Gao, F.; Goodman, D. Pd-Au Bimetallic Catalysts: Understanding Alloy Effects from Planar Models and (Supported) Nanoparticles. *Chem. Soc. Rev.* **2012**, *41*, 8009–8020.